

Reduced forms of the Wigner distribution function for the numerical analysis of rotationally symmetric synchrotron radiation

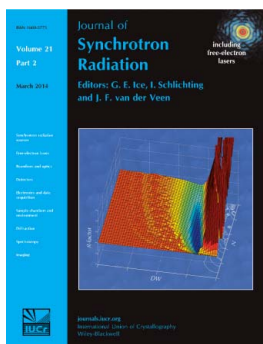
Andrew Gasbarro and Ivan Bazarov

J. Synchrotron Rad. (2014). **21**, 289–299

Copyright © International Union of Crystallography

Author(s) of this paper may load this reprint on their own web site or institutional repository provided that this cover page is retained. Republication of this article or its storage in electronic databases other than as specified above is not permitted without prior permission in writing from the IUCr.

For further information see <http://journals.iucr.org/services/authorrights.html>



Synchrotron radiation research is rapidly expanding with many new sources of radiation being created globally. Synchrotron radiation plays a leading role in pure science and in emerging technologies. The *Journal of Synchrotron Radiation* provides comprehensive coverage of the entire field of synchrotron radiation research including instrumentation, theory, computing and scientific applications in areas such as biology, nanoscience and materials science. Rapid publication ensures an up-to-date information resource for scientists and engineers in the field.

Crystallography Journals **Online** is available from journals.iucr.org

Reduced forms of the Wigner distribution function for the numerical analysis of rotationally symmetric synchrotron radiation

Andrew Gasbarro and Ivan Bazarov*

Cornell University, Ithaca, NY 14853, USA. *E-mail: ib38@cornell.edu

In an effort to provide a computationally convenient approach to the characterization of partially coherent synchrotron radiation in phase space, a thorough discussion of the minimum dimensionality of the Wigner distribution function for rotationally symmetric sources of arbitrary degrees of coherence is presented. It is found that perfectly coherent, perfectly incoherent and partially coherent sources may all be characterized by a three-dimensional reduced Wigner distribution function, and some special cases are discussed in which a two-dimensional reduced Wigner distribution function suffices. An application of the dimension-reducing formalism to the case of partially coherent radiation from a planar undulator and a circularly symmetric electron beam as can be found in linear accelerators is demonstrated. The photon distribution is convolved over a realistic electron bunch, and how the beta function, emittance and energy spread of the bunch affect the total degree of coherence of the radiation is inspected. Finally the cross spectral density is diagonalized and the eigenmodes of the partially coherent radiation are recovered.

Keywords: brightness; coherence; Wigner distribution function; emittance; radial symmetry; undulator radiation.

© 2014 International Union of Crystallography

1. Introduction

In an effort to simulate synchrotron radiation sources (non free-electron laser), a full numerical characterization of partially coherent sources has shown itself to be a topic of some debate. In recent work, Vartanyants & Singer (2010) have shown that the Gauss–Schell model can be sufficient to characterize certain undulator sources. Geloni *et al.* (2008) have argued that the Gauss–Schell model does not properly describe the coherence properties of non-homogeneous undulator sources. In this work, we forgo the use of Gauss–Schell and other approximate models and provide a method for computing the Wigner distribution function (WDF) (or, equivalently, the cross spectral density) directly from the electron bunch distribution.

In general, complete characterization of a partially coherent source is a difficult computational challenge. One avenue is to compute the electric fields produced by each of the different electrons in a bunch and to sum these fields incoherently (Chubar *et al.*, 2002). Another approach is to study the radiation in phase space using the Wigner distribution function (Bazarov, 2012). In phase space, incoherent superpositions amount to sums of WDFs, and under appropriate conditions incorporation of the electron bunch effect may be accomplished by a simple convolution. Another advantage of working in phase space is that the WDF may be interpreted

physically as a generalized brightness. Though the WDF takes on negative values for non-Gaussian sources, the WDF may be measured uniquely using tomographic techniques (Smithey *et al.*, 1993; Tran, 2007). The WDF, of course, has its limitations; for example, when used with beam transport that includes non-linear optics (aberrations) and spatial filters.

For a general linearly polarized paraxial source, the WDF at a given radiation frequency is a four-dimensional (4D) object, which can be cumbersome to work with computationally. However, the dimensionality of the WDF may be reduced if the system exhibits rotational symmetry (Alieva & Bastiaans, 2000). Taking advantage of the symmetry of a rotationally symmetric system minimizes the computational burden by reducing the dimension of the WDF from 4D to 3D.

Undulator radiation from a single ('zero' emittance) electron beam displays a highly circular nature at odd harmonics. Thus, to take full advantage of transverse coherence properties, electron beams should be naturally circular as well. Even though present day storage rings display large asymmetry in horizontal *versus* vertical emittances, a proposed energy-recovery linac (ERL) source (Bartnik *et al.*, 2013) as well as ultimate storage ring designs tend to have nearly round beams (Borland, 2013) with roughly equal emittances. Therefore the techniques utilizing rotational symmetry presented in this paper should prove useful for the analysis of next-generation synchrotron radiation sources.

The purpose of this paper is to provide a thorough discussion of the minimum dimensionality of the Wigner distribution function for rotationally symmetric sources and to demonstrate how these concepts can be applied to the difficult computational problem of characterizing partially coherent undulator radiation. Depending on the nature of a model, it is often, as we shall see in our case, necessary to understand how the dimensionality of the WDF may be reduced for a source of arbitrary degree of coherence. In §2 we shall discuss in detail how perfectly coherent, partially coherent and perfectly incoherent sources may be described by reduced forms of the WDF when rotational symmetry is assumed. We shall demonstrate that a large class of systems of arbitrary degrees of coherence may be fully characterized by a WDF of three or fewer dimensions. In §3, we shall apply the concepts developed in §2 to a model of partially coherent planar undulator radiation. We will demonstrate how to appropriately characterize the source in a 3D reduced phase space and how a full characterization of the system allows us to compute the total degree of coherence and to perform orthogonal mode decomposition.

2. Reduced forms of the Wigner distribution function

In this section we will introduce a formalism for reducing the dimension of the WDF of rotationally symmetric sources of any degree of coherence. First we will need to define the basic quantities that we will be working with.

2.1. Basic definitions

Let us reproduce the expression for the WDF of a scalar frequency domain electric field. When applied to light, the WDF may be normalized to units of brightness in analogy with a density of states of classical rays (Kim, 1989),

$$B(\mathbf{r}, \boldsymbol{\theta}) = \frac{2c\epsilon_0 I}{h\lambda^2 e} \int_{-\infty}^{\infty} d^2\mathbf{r}' \times W[\mathbf{r} - (\mathbf{r}'/2), \mathbf{r} + (\mathbf{r}'/2)] \exp(ik\mathbf{r}' \cdot \boldsymbol{\theta}). \quad (1)$$

c is the speed of light, ϵ_0 is the vacuum permittivity, e is the electron charge and h is Planck's constant. λ and k are the wavelength and wavenumber of the radiation. I is the average electron beam current, and W is the cross spectral density (CSD), *i.e.* the optical analog of the density matrix from quantum mechanics. For a monochromatic pure mode,

$$W(\mathbf{r}_1, \mathbf{r}_2) = E(\mathbf{r}_1) E^*(\mathbf{r}_2), \quad (2)$$

where we have considered only the transverse spatial dependence of the fields. The monochromatic field with frequency ω is measured on a detector with fixed longitudinal position, z : $E(\mathbf{r}) \equiv E(\mathbf{r}; z; \omega)$.

For the treatment of vector fields (polarization), there is an extension of equation (1) which requires four WDFs referred to as 'generalized Stokes parameters' to describe an arbitrarily polarized source (Luis, 2005). This method is well understood, so we shall constrain our discussion to scalar fields and a single

WDF, which are sufficient to characterize linearly polarized sources such as planar undulator radiation.

Equation (1) is fully invertible such that there is a 1:1 correspondence between the WDF and the CSD (*e.g.* see Bazarov, 2012),

$$W(\mathbf{r}_1, \mathbf{r}_2) = \int_{-\infty}^{\infty} d^2\boldsymbol{\theta} B\left(\frac{\mathbf{r}_1 + \mathbf{r}_2}{2}, \boldsymbol{\theta}\right) \exp[ik(\mathbf{r}_1 - \mathbf{r}_2) \cdot \boldsymbol{\theta}]. \quad (3)$$

Equations (1) and (3) together are known as Wigner–Weyl transformations, and they tell us that the WDF and CSD are in fact the same operator viewed in phase space and position space, respectively. It is a matter of preference in which space one chooses to work. In this paper we opt to work primarily in phase space, and we will motivate this decision in §3

Note that, by setting $\mathbf{r}_2 = 0$ in (2), one recovers the electric field up to a complex constant. It follows that there is a 1:1 correspondence between the WDF and the electric field (up to a complex constant) for a pure mode. For an extended discussion of the WDF in application to synchrotron radiation, see Bazarov (2012).

In this paper we are interested in analyzing the degree of coherence of the frequency domain fields over space; we will not treat temporal coherence in this work. The appropriate quantity for doing this is the complex spectral degree of coherence. Given in terms of the CSD (Goodman, 2000; Luis, 2007),

$$\mu(\mathbf{r}_1, \mathbf{r}_2) = \frac{W(\mathbf{r}_1, \mathbf{r}_2)}{[W(\mathbf{r}_1, \mathbf{r}_1)W(\mathbf{r}_2, \mathbf{r}_2)]^{1/2}}. \quad (4)$$

Here, $\mu(\mathbf{r}_1, \mathbf{r}_2)$ is a complex quantity with amplitude from zero to one, and it is related to the visibility. In the case of full transverse coherence, $\mu(\mathbf{r}_1, \mathbf{r}_2) = 1$ everywhere, which is the case for a pure radiation mode produced by a zero-emittance electron beam.

As in Luis (2007), we take the norm-square of μ and average over space to find the overall spectral degree of coherence (squared), μ_g^2 . μ_g^2 may be computed *via* the CSD (Luis, 2007),

$$\mu_g^2 = \frac{\int d^2\mathbf{r}_1 d^2\mathbf{r}_2 |W(\mathbf{r}_1, \mathbf{r}_2)|^2}{|\int d^2\mathbf{r} W(\mathbf{r}, \mathbf{r})|^2} \quad (5)$$

or the WDF (Luis, 2007),

$$\mu_g^2 = \frac{\int d^2\mathbf{r} d^2\boldsymbol{\theta} B(\mathbf{r}, \boldsymbol{\theta})^2}{[\int d^2\mathbf{r} d^2\boldsymbol{\theta} B(\mathbf{r}, \boldsymbol{\theta})]^2}. \quad (6)$$

μ_g^2 will be our measure of coherence in this paper, and we will refer to it as simply the overall degree of coherence.

As will be shown later, the undulator radiation in the central cone from a single electron displays rotational symmetry. The advent of linac-based synchrotron radiation sources, where electron beams are also mostly radially symmetric, motivates the following discussion. Let us introduce a useful set of polar coordinates,

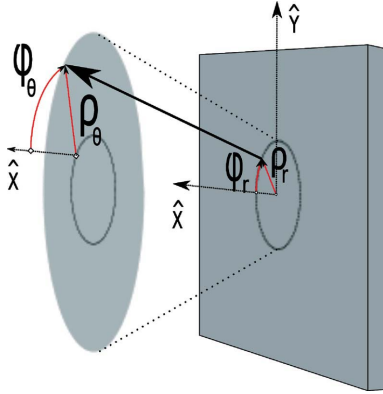


Figure 1
A ray specified by polar coordinates.

$$\begin{aligned} x &= \rho_r \cos(\varphi_r), \\ y &= \rho_r \sin(\varphi_r), \\ \theta_x &= \rho_\theta \cos(\varphi_\theta), \\ \theta_y &= \rho_\theta \sin(\varphi_\theta). \end{aligned} \quad (7)$$

Fig. 1 demonstrates how these coordinates describe a ray in real space. Though the WDF is not a phase space distribution in the classical statistical sense, it is still often useful to think of it in terms of rays.

Next, let us discuss the reduced forms of the WDF. The case of perfectly coherent beams which are symmetric under spatial rotation has been discussed elsewhere (Alieva & Bastiaans, 2000). However, their discussion is not exhaustive, and we seek to understand the minimum dimensionality of the WDF under rotational symmetry for sources of arbitrary degree of coherence. We shall see in §3 that this is necessary to numerically represent our model for partially coherent planar undulator radiation from a linac-based electron beam.

2.2. Perfectly coherent radiation

A perfectly coherent source is characterized by a single electric field such that its CSD is of the form given by equation (2). In general, we must allow a rotationally symmetric complex field to pick up a global phase. Thus under a spatial rotation, $R(\gamma)$, the most general transformation of a rotationally invariant field is

$$E(\mathbf{r}) \xrightarrow{R(\gamma)} E(\mathbf{r}) \exp(i\ell\gamma). \quad (8)$$

Fields exhibiting this behavior take the form

$$E_l(\mathbf{r}) = R(\rho_r) \exp[i\psi(\rho_r)] \exp(i\ell\varphi_r). \quad (9)$$

ℓ must take on integer values in order to satisfy periodic boundary conditions in φ_r . Fields exhibiting helical wavefronts ($\ell > 0$) are called ‘twisted modes’. It can be seen that the fields in equation (9) are eigenmodes of the orbital angular momentum operator, $L_z = -i\hbar/(2\pi)\partial/\partial\varphi_r$.

2.2.1. 2D representations. When $\ell = 0$, the field does not pick up an additional phase after rotation, and we call the mode ‘non-twisted’. For these fields, $E(\mathbf{r}) = E(\rho_r)$, which is to say that the real and imaginary parts of the field are each

rotationally symmetric. A rotational symmetry implies one less degree of freedom, so one would expect that the WDF for non-twisted fields would be two-dimensional. A 2D WDF may be constructed from the one-dimensional field sample along a radial line, $E(\rho_r = r, \varphi_r = \varphi_{r0}) \leftrightarrow W_r(r, \theta_r)$, from which the full 4D WDF may be recovered (Agarwal & Simon, 2000). However, this 2D WDF will not return the correct electric field after being propagated through simple drifts because the Fresnel diffraction in one transverse dimension does not equate to diffraction in a rotationally symmetric system of two transverse dimensions. A simple example here is the diffraction pattern for a 1D slit *versus* a 2D disk; the former is a sinc function and the latter is an Airy function. Therefore, although a non-twisted rotationally symmetric mode only consists of two degrees of freedom worth of information, we have not found a convenient manifestation of this fact to allow for a useful 2D representation in phase space.

One special case that can be treated in 2D is separable modes. When the electric field separates as $E(\mathbf{r}) = E_x(x)E_y(y)$, the WDF separates accordingly,

$$B(\mathbf{r}, \boldsymbol{\theta}) = B_x(x, \theta_x) B_y(y, \theta_y). \quad (10)$$

B_x and B_y are the 2D WDFs of E_x and E_y , respectively. In this case, the most meaningful 2D representation in phase space amounts to a projection of a higher dimensional WDF, and the 4D WDF is simply an outer product of two projections. It follows from (10) that any dynamics which do not couple x and y , such as simple drifts, cylindrical lenses and radially symmetric lenses, may be equivalently carried out *via* the 2D WDFs. Also, one may compute μ_g^2 , equation (6), for a separable mode as a product of expressions involving the 2D WDFs,

$$\mu_g^2 = \frac{\int B_x^2(x, \theta_x) dx d\theta_x \int B_y^2(y, \theta_y) dy d\theta_y}{[\int B_x(x, \theta_x) dx d\theta_x]^2 [\int B_y(y, \theta_y) dy d\theta_y]^2}. \quad (11)$$

In this way, the treatment of separable modes in 2D phase space can greatly simplify calculations.

2.2.2. 3D representations. We have already seen that although non-twisted modes have only two degrees of freedom, they cannot be usefully represented by a 2D WDF. We will now show by example that twisted modes have three degrees of freedom, so there is no chance that a 2D representation will suffice. Thus, all modes of the form of equation (9) will be represented by 3D WDFs.

One can obtain a rough picture of the twistedness of rays by looking at the averaged cross section $B_{av}(x, \theta_y) \equiv \int d\theta_x B(x, 0, \theta_x, \theta_y)$. That is, by taking the cross section along a radial line (in this case, $y = 0$) and then averaging over radial momenta. This gives a rough picture of tangential momentum *versus* radius. Fig. 2 shows cross sections of the WDF from Laguerre–Gauss (LG) modes with $\ell = 0$ and $\ell > 0$. Notice how with non-zero orbital angular momentum comes an additional asymmetry in the tangential momentum (θ_y) about the radial line (x). For $\ell > 0$, there is a net propagation of rays off their radial line. This corresponds to a new degree of freedom which did not exist in the non-twisted case, and therefore the twisted modes here have three degrees of freedom.

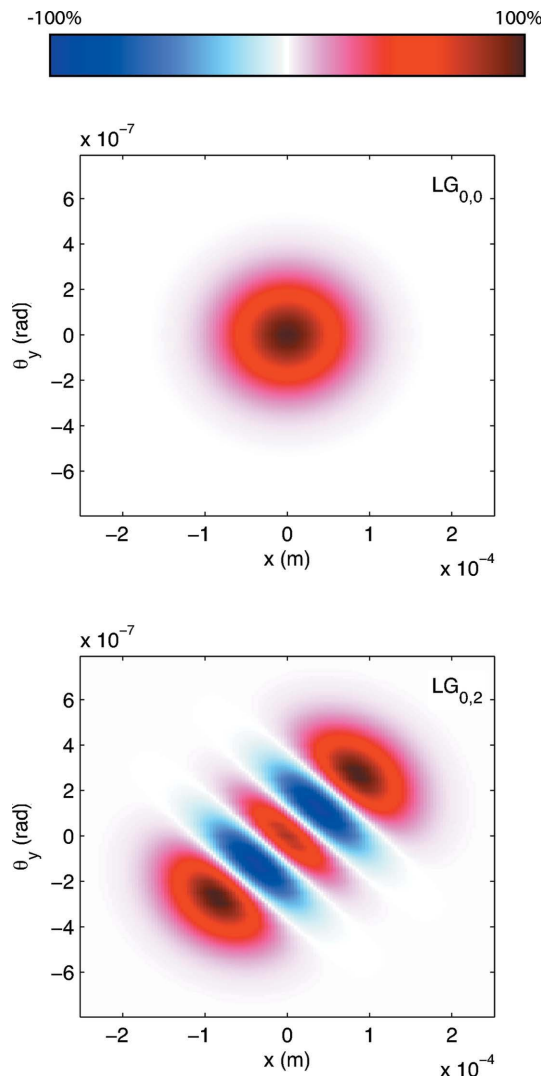


Figure 2
 $B_{av}(x, \theta_y)$ demonstrating twistedness in LG_{00} (top) and LG_{02} (bottom). The fields are computed at the waist, $z = 0$, and the waist size is specified to be $w_0 = 100 \mu\text{m}$. The wavelength is $\lambda = 1 \text{ \AA}$. In the chosen color map, white corresponds to zero, dark red corresponds to large positive values, and dark blue corresponds to large negative values.

The 3D WDF is defined *via* a dimension-reducing condition on the 4D WDF. Alieva & Bastiaans (2000) have shown that a dimension-reducing condition may be derived directly from the WDF definition when $E(\mathbf{r}) = E(|\mathbf{r}|)$. We show in Appendix A that this condition can be proven to hold for all fields of the form of equation (9). In rectangular coordinates, this result can be written as

$$B \begin{pmatrix} x \\ y \\ \theta_x \\ \theta_y \end{pmatrix} = B \begin{pmatrix} x \cos(\gamma) - y \sin(\gamma) \\ y \cos(\gamma) + x \sin(\gamma) \\ \theta_x \cos(\gamma) - \theta_y \sin(\gamma) \\ \theta_y \cos(\gamma) + \theta_x \sin(\gamma) \end{pmatrix}, \quad (12)$$

which holds for any rotation angle γ . The coordinates have been placed into columns only to condense the notation. This relationship implies that the full four-dimensional distribution may be recovered from any three-dimensional slice *via* inter-

polation. We typically choose to work with the slice $y = 0$ by setting $\gamma = -\text{atan}(y/x)$, which gives the recovery condition

$$B \begin{pmatrix} x \\ y \\ \theta_x \\ \theta_y \end{pmatrix} = B \begin{pmatrix} (x^2 + y^2)^{1/2} \\ 0 \\ (x\theta_x + y\theta_y)/(x^2 + y^2)^{1/2} \\ (x\theta_y - y\theta_x)/(x^2 + y^2)^{1/2} \end{pmatrix}. \quad (13)$$

These will be our most important equations for working with the reduced-dimension WDF.

2.3. Perfectly incoherent radiation

In the limit of perfect incoherence, radiation fields reduce to classical geometrical rays, electron wavefunctions reduce to point particles, and the Wigner function reduces to a classical density of states (or, more exactly, its Fourier transform). The uncertainty principle for ultra-relativistic electrons gives tiny zero-like emittances as compared with the radiation wavelength, so the electrons behave like point particles. In this paper we treat the electron bunch as a perfectly incoherent source. We now briefly discuss the behavior of a classical distribution under rotational invariance.

2.3.1. 3D representations. For a classical ray described by polar coordinates (Fig. 1), φ_r and φ_θ vary together under spatial rotation such that their difference is always unchanged. Therefore, for a rotationally symmetric system the transformation $\varphi_r \rightarrow \varphi_r + \gamma$ and $\varphi_\theta \rightarrow \varphi_\theta + \gamma$ must leave the WDF unchanged. In Cartesian coordinates, this is exactly the symmetry relation we found for the perfectly coherent case, equation (12). Therefore any rotationally symmetric perfectly incoherent source may be represented by a 3D WDF in the same manner that we have shown for the perfectly coherent case. Three degrees of freedom remain because rays still have two momentum degrees of freedom and one spatial degree of freedom. The position and momenta of rays along a radial line may be arbitrary distributed as long as the distribution along each radial line is the same. This leaves open the possibility of a net orbital angular momentum (the so-called ‘magnetized beams’).

2.3.2. 2D representations. As in the perfectly coherent case, if the tangential ray momenta are symmetrically distributed about a radial line, the source will have no net orbital angular momentum (non-twisted). For the perfectly coherent case, this allowed us to consider a 2D WDF constructed from the radial field sample. The same is not possible for incoherent sources because there is no field to speak of.

In the special case where rays only propagate radially, the WDF becomes 2D in the sense that all information is given on a 2D sheet inside of 4D phase space,

$$B \begin{pmatrix} \rho_r \\ \varphi_r \\ \rho_\theta \\ \varphi_\theta \end{pmatrix} = \begin{cases} 0 & \text{if } \varphi_r \neq \varphi_\theta, \\ B \begin{pmatrix} \rho_r \\ 0 \\ \rho_\theta \\ 0 \end{pmatrix} & \text{otherwise,} \end{cases} \quad (14)$$

but ray distributions like this are only produced from point sources, *i.e.* sources with zero emittance. Fig. 3 shows how a

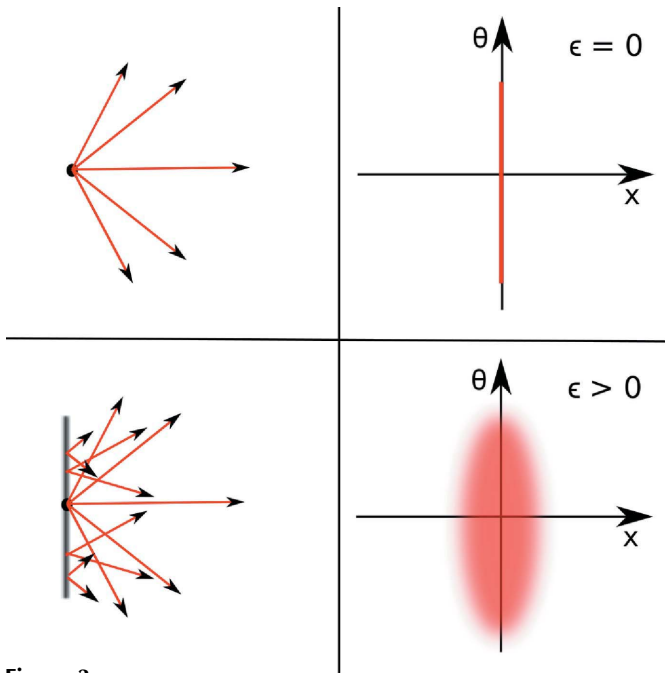


Figure 3 Demonstrating a zero emittance (top) and a non-zero emittance (bottom) source in real space (left) and phase space (right). Only the zero emittance source is able to produce light with only radially propagating rays.

zero-emittance source produces radially propagating rays. However, for even a well behaved extended source (emittance greater than zero), there will always be rays propagating off of radial lines. Thus we conclude that, for any perfectly incoherent rotationally symmetric source of non-zero emittance, the minimum dimensionality of the WDF is still 3D.

2.4. Partially coherent radiation

So far we have seen that a 2D WDF will only suffice in special cases of perfectly coherent and perfectly incoherent rotationally symmetric sources, none of which are instrumental for a realistic simulation of synchrotron radiation. For the more complicated case of partially coherent sources, we limit the subsequent discussion to cases when a 3D representation is appropriate.

Partially coherent radiation cannot be represented by a single field or visualized by geometrical rays. The radiation consists of a collection of pure modes that are distributed by a classical probability distribution. In quantum mechanics, these systems are known as mixed states and are described by density matrices (see, for example, Sakurai & Napolitano, 2010). The CSD is the optical analog to the density matrix (Bazarov, 2012). It is always possible to decompose the CSD into a set of orthogonal modes,

$$W(\mathbf{r}_1, \mathbf{r}_2) = \sum_n \lambda_n \varphi_n(\mathbf{r}_1) \varphi_n^*(\mathbf{r}_2), \quad (15)$$

where the eigenvalue λ_n is the new relative weight of the pure mode φ_n , and $\{\varphi_n\}$ is the orthogonal eigenbasis of W . There still exists a 1:1 correspondence between the WDF and the CSD, which are related by equations (1) and (3), so the WDF is an

equally appropriate description of the partially coherent radiation. It follows from (1) and (15) that the WDF of a partially coherent source is a weighted sum of pure mode WDFs.

There are two cases when the WDF for the partially coherent radiation is guaranteed to be reducible, *i.e.* obey equation (12). First, when the pure modes making up the density matrix (15) have the form of equation (9), then the total WDF will be a sum of pure mode WDFs obeying equation (12), and so the total WDF will as well. Second, it can be shown that the convolution of two WDFs obeying equation (12) will also obey that symmetry. We shall see in §3 that our model for partially coherent synchrotron radiation will be a convolution of a perfectly coherent distribution and a perfectly incoherent distribution each obeying equation (12).

3. Characterization of realistic synchrotron radiation sources

Here we will demonstrate an application of using the 3D WDF for a complete characterization of partially coherent radially symmetric undulator radiation. We seek to compute and analyze an object containing all physics of the partially coherent radiation produced by many electrons.

One may choose to work with the CSD instead of the WDF for analysis of partially coherent radiation. There is a 1:1 correspondence between the WDF and the CSD *via* the Wigner–Weyl transformation equations (1) and (3). Furthermore, if the WDF obeys the dimension-reducing condition (12), there is a corresponding dimension-reducing condition in the CSD (see Appendix B for proof),

$$W \begin{pmatrix} x_1 \\ y_1 \\ x_2 \\ y_2 \end{pmatrix} = W \begin{pmatrix} x_1 \cos \gamma - y_1 \sin \gamma \\ y_1 \cos \gamma + x_1 \sin \gamma \\ x_2 \cos \gamma - y_2 \sin \gamma \\ y_2 \cos \gamma + x_2 \sin \gamma \end{pmatrix}. \quad (16)$$

Then one would compute the reduced CSD by summing over single electron fields with a statistical weight factor ρ that specifies the electron bunch distribution,

$$W(x_1, y_1, x_2) = \sum_i \rho_i E_i(x_1, y_1) E_i^*(x_2, 0). \quad (17)$$

E_i produced by an electron displaced off-axis would differ from the field produced by an on-axis electron by a translation. If the off-axis electron was deflected, it would produce fields with additional linear phase fronts. These fields could be computed, and the sum in (17) could be performed, but the authors find it more appealing to work in phase space.

We choose to work with the WDF for two reasons. First, in phase space each dimension corresponds to a degree of freedom, so when we reduce the dimension of the space it is clear that this is possible because there are fewer degrees of freedom. Second, an electron bunch that is distributed in position and momentum produces our radiation source, and it is most natural to describe this bunch in phase space. Then the WDF of the partially coherent radiation is computed *via* a simple convolution over phase space as we shall discuss.

Table 1

Undulator, beam and radiation parameters.

Number of periods	N_u	1250
Undulator spatial period	λ_u	2 cm
Photon energy	$E_{\text{ph}0}$	8000 eV
Beam energy	E	5 GeV
Average current	I	100 mA
Detector position	z_0	75 m
Undulator parameter	K	0.9839

The following techniques will only apply for fields obeying equation (9) and WDFs obeying equation (12). To model the radiation, we will first compute the radiation field produced by a single electron and compute the reduced WDF of these fields. We will incorporate an electron bunch with non-zero emittance by modeling the bunch by a rotationally symmetric distribution in classical phase space. The undulator parameters that we use for our example are given in Table 1. The parameters chosen for this example are close to those for the proposed Cornell ERL (Bartnik *et al.*, 2013).

The coherent radiation fields produced by a single electron in an undulator may be computed numerically by solving Maxwell's equations or from analytical formulae given by Kim (1989). We use symplectic integration techniques to compute the fields numerically, and find that they are in good accordance with equation (9). For more details on the numerical computation of fields, see Bazarov & Gasbarro (2012).

Kim (1989) gives the far-field pattern for the undulator radiation,

$$\mathcal{E}_{\sigma,\pi}(\varphi, \psi) \propto s_n(\theta) B_{\sigma,\pi}(\varphi, \psi), \quad (18)$$

$$s_n = \sin[N_{\text{und}} \pi \omega / \omega_1(\theta)] / \sin[\pi \omega / \omega_1(\theta)], \quad (19)$$

$$\begin{pmatrix} B_\sigma \\ B_\pi \end{pmatrix} = \frac{1}{\pi} \int_{-\pi}^{\pi} d\xi \begin{pmatrix} \varphi/K - \cos \xi \\ \psi/K \end{pmatrix} \times \exp(i\{\omega/\omega_1(\theta)\xi - p \sin \xi + q \sin 2\xi\}), \quad (20)$$

where $\{\hat{\sigma}, \hat{\pi}\}$ is a rotated coordinate system, and $\mathcal{E}_x \simeq \mathcal{E}_\sigma$ for small angles. $\theta = (\varphi^2 + \psi^2)^{1/2} = \text{atan}(r/z)$ is a radial parameter such that a function of θ alone is exactly rotationally symmetric. Functions in which φ and ψ vary independently are in general not rotationally symmetric. For more details on the coordinate system, see Kim (1989). The angular dependence of the resonance frequency which enters equation (18) is given by the undulator equation,

$$\omega_1(\theta) = \frac{\omega_1(0)}{1 + [\gamma^2 \theta^2 / (1 + K^2/2)]}, \quad (21)$$

where K is the undulator parameter and γ is the relativistic factor.

Over a range of $\varphi, \psi \simeq 1/\gamma$, the variation in $B_{\sigma,\pi}$ is slow varying compared with s_n . Thus one can treat $B_{\sigma,\pi}$ to be constant to good approximation such that $\mathcal{E}_{\sigma,\pi}(\varphi, \psi) \propto s_n(\theta)$ is rotationally symmetric. The approximation applies only for odd harmonics. For even harmonics, B_π goes to zero on-axis, and so its effect is not negligible. Kim (1986, 1989) computes

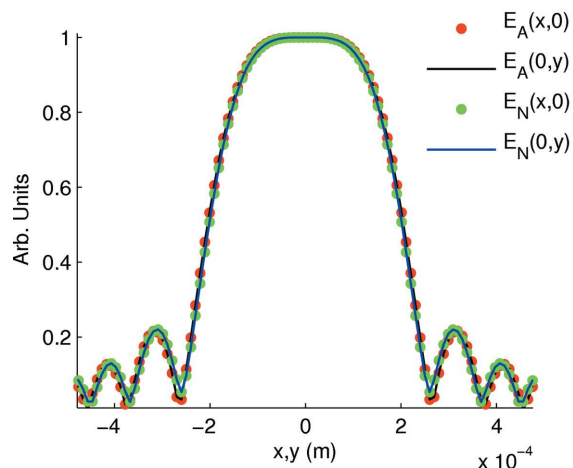


Figure 4

Undulator radiation electric field amplitude computed numerically (E_N) and analytically (E_A). Slices are shown at $x = 0$ and $y = 0$ to demonstrate rotational symmetry.

the WDF under this approximation, and it can be seen from his expression that the WDF obeys equation (12).

Fig. 4 shows slices of the radiation fields computed numerically and analytically. Both the numerically and analytically computed fields demonstrate rotational symmetry in that $E(x, 0) \simeq E(0, y)$. The discrepancy between the analytical and numerical fields arises from the fact that the analytical fields do not take into account the tuning of the pole magnets at the ends of the undulator to keep the electron trajectories on-axis. The numerical computation does include this and so the fields vary slightly.

We note that helical undulators are rotationally symmetric sources which carry circular polarization, and therefore they may be treated using the formalism of §2 in combination with generalized Stokes parameters (Luis, 2005). The higher harmonics, which are known to carry orbital angular momentum (Afanasev & Mikhailichenko, 2011) as well as spin angular momentum, have the form of equation (9), and so they may also be represented by a 3D-reduced WDF.

3.1. Convolution with electron beam distribution

Here we will demonstrate the effects of non-zero energy spread and non-zero emittance in the electron bunch on the phase space profile of the partially coherent radiation. It is often considered that $\lambda/4\pi$ diffraction-limited emittance of the electron beam is sufficient to obtain transverse coherence. It should be noted that synchrotron radiation from an undulator is not Gaussian and therefore X-ray light emittance from perfect (zero emittance) electron beam differs from $\lambda/4\pi$ (Bazarov & Gasbarro, 2012). Beam energy spread also plays a role. In §3.2 we investigate this question quantitatively in some detail and show that for electron beam emittance of $\lambda/4\pi$ and energy spread $1/N_{\text{und}}$ the overall degree of coherence μ_g^2 still significantly differs from 1.

Fig. 5 demonstrates how the phase space profile of the radiation changes as we convolve over the electron bunch. The

electron energy is normally distributed with standard deviation $\sigma_E/E = 1/(4N_{\text{und}})$ and the bunch emittance is $\varepsilon = \lambda/(4\pi)$. It is well established that, to good approximation, the WDF of photons produced by an electron bunch passing through a magnetic field structure may be computed by convolving the WDF of photons produced by a single electron, B_{ph} , with the WDF of the electron bunch distribution, B_e . The fields produced by a single relativistic electron are determined for an arbitrary trajectory by Maxwell's equations, so B_{ph} is perfectly coherent. The electron bunch is modeled as a statistical distribution of classical particles, so B_e is perfectly incoherent. The total WDF is given by

$$B_{\text{tot}} = B_{\text{ph}} * B_e, \quad (22)$$

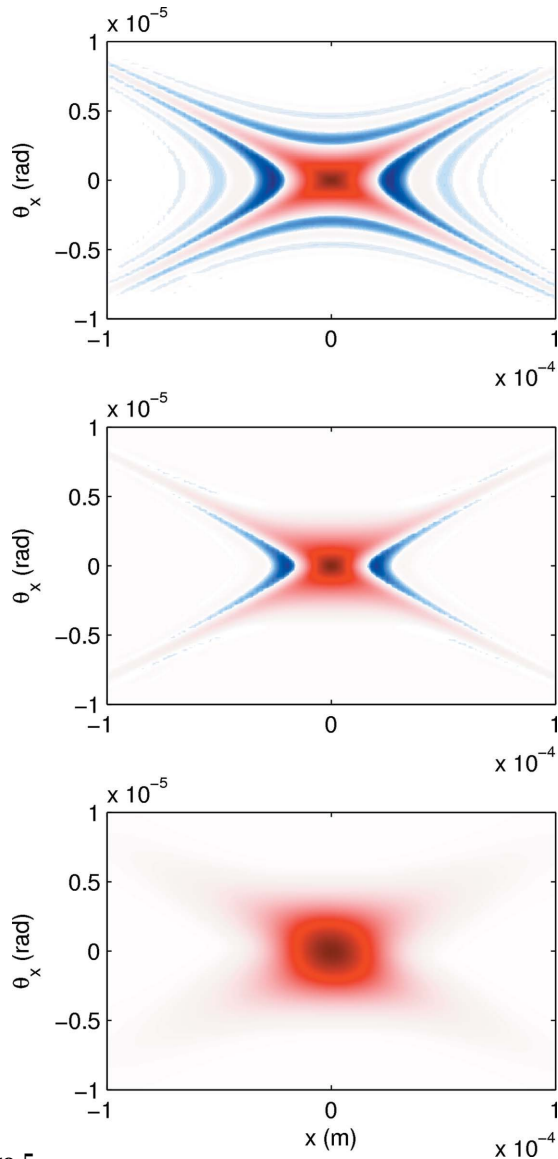


Figure 5 WDF for undulator radiation. Top: single electron. Center: non-zero energy bandwidth bunch. Bottom: non-zero energy bandwidth and non-zero emittance bunch. The color map is such that dark red corresponds to large positive values, and dark blue corresponds to large negative values (as in Fig. 2).

where $*$ is the convolution operator. B_{tot} is a partially coherent photon distribution. Note that the WDF is bilinear in the fields, and so adding Wigner distributions, like adding intensities, is an incoherent superposition.

Any model for the transverse profile of the electron bunch obeying equation (12) will work. We choose to work with a Gaussian density of states, which is specified by a single set of Twiss parameters and a single emittance,

$$B(\mathbf{r}, \boldsymbol{\theta}) = B_0 \exp\left[-\left(\frac{\gamma \mathbf{r}^2 + 2\alpha \mathbf{r} \cdot \boldsymbol{\theta} + \beta \boldsymbol{\theta}^2}{2\varepsilon}\right)\right]. \quad (23)$$

The model equation (22) applies only when the Wigner of photons produced by off-axis electrons does not differ much from the WDF of photons produced by an on-axis electron. For an electron displaced parallel to the plane of the undulator (what we will call the ‘ x ’ direction, normally in the horizontal plane), there will be no non-linear effects because the electron bunch is very small compared with the size of the magnets.

For electrons displaced perpendicular to the undulator plane (the ‘ y ’ direction), there are two non-linear effects to consider. First, the magnetic field strength experienced by the electron has a $\cosh^2(ky)$ dependence such that an electron displaced in y will experience a stronger magnetic field leading to a shift of the electric field resonance (Bazarov & Gasbarro, 2012). Second, undulator fields have a weak lensing effect for electrons displaced in y which pulls them back toward the axis. These effects may play an important role in certain cases, but for high-brightness electron beams we have found both of these effects to be negligible.

In convolving over the electron energy spread, the WDF of radiation from a single electron does vary appreciably with electron energy, so the energy convolution is performed with ‘brute force’, *i.e.* the radiation fields are computed many times for electrons of various energies, and the 3D WDFs of each of the fields are computed and then summed according to some weighing function. Again, we choose a Gaussian energy profile centered at E with standard deviation $\sigma_E = E/(4N_{\text{und}})$. We note that an energy spread in the electron beam is related to a spread in angles due to the relativistic Doppler effect; the size of the central cone varies as $1/\gamma$. Also, the resonant wavelength $\lambda_r \propto 1/\gamma^2$, so a spread in the electron beam energy is related to a blurring of frequencies around resonance. Nonetheless, experimentally the situation amounts to having a perfect monochromator downstream from the undulator.

In computing the 4D convolution over the electron bunch distribution, we avoid 4D arrays by exploiting equations (12) and (13) and computing the 3D slice of the convolved distribution at $y = 0$,

$$B_{\text{tot}}\left(\begin{array}{c} x \\ y=0 \\ \theta_x \\ \theta_y \end{array}\right) = \int dy' \mathcal{C}\left\{B_{\text{ph}}\left(\begin{array}{c} x \\ y' \\ \theta_x \\ \theta_y \end{array}\right), B_e\left(\begin{array}{c} x \\ -y' \\ \theta_x \\ \theta_y \end{array}\right)\right\}_{x,\theta_x,\theta_y}. \quad (24)$$

$\mathcal{C}\{A, B\}_{a_1, \dots, a_n}$ denotes the convolution of the functions A and B over the variables a_1, \dots, a_n . The fully convolved WDF is

easily computed *via* this formula by invoking equation (13). Fig. 5 shows the WDF projected into 2D during various stages of the convolution. Notice that, after convolution over the electron bunch, the phase space of the radiation remains distinctly non-Gaussian.

3.2. Optimization of electron beam parameters

It is well known that phase space profiles of the electron bunch and the photons produced by a single electron should be matched, but which electron beam parameters maximize coherence? With access to the full WDF of the partially coherent undulator radiation, we are in a position to inspect directly the impact of electron beam parameters on the overall degree of coherence, μ_g^2 . μ_g^2 is computed from the WDF by equation (6). To compute the numerator of this expression, many 3D slices are recovered using equation (12) and are summed over in such a way that 4D arrays are never required.

As in §3.1, we consider an example of radiation produced by an electron bunch with Gaussian phase space distribution and Gaussian energy distribution. Let us denote the emittance of the electron bunch profile by ε_e , the electron beta function by β_e , and the standard deviation of the energy distribution is σ_E . In Fig. 6(a), $\varepsilon_e = 0$ and σ_E varies. In Fig. 6(b), $\sigma_E = 0$ and β_e is held fixed to match the β -function of the photon distribution produced by a single electron, β_{ph} , while ε_e varies. In Fig. 6(c), $\sigma_E = 0$, $\varepsilon_e = \lambda/(4\pi)$ and β_e varies.

Naturally, coherence will always decrease with increased electron bunch emittance and electron energy spread. Figs. 6(a) and 6(b) demonstrate precisely how quickly coherence is lost as emittance and energy bandwidth increase while all else is held fixed. Fig. 6(c) illustrates the dependence of μ_g^2 on the electron bunch β -function, β_e , with emittance and energy bandwidth held fixed. Analyses of this kind are significant for the design of beamlines when seeking to produce highly coherent radiation from insertion devices. The β -function which maximizes coherence varies with electron beam and undulator parameters, and the explicit calculation

shown in Fig. 6(c) is necessary to find the optimal β -function value for a particular system.

3.3. Modal decomposition

With the full WDF that we have computed, we are able to decompose partially coherent undulator radiation into its constituent modes. In order to do this, we recover the CSD from the WDF *via* equation (3) and then diagonalize. In order to perform this diagonalization, we unfold the 3D CSD into a 4D array. The question of whether this diagonalization can be done entirely in 3D remains open.

Fig. 7 shows the first two modes after a convolution over the energy bandwidth. Only two modes are given because the eigenvalue of the third mode is smaller than the numerical error, so this mode cannot be trusted to be accurate. Even if the error were reduced, the contribution of additional modes to the radiation would be insignificant compared with the two modes given. The rapidity with which the eigenvalues fall off illustrates that the source is still fairly coherent after only an energy convolution. Fig. 8 shows the first few modes after convolution over energy bandwidth and spatial bunch distribution. Notice how more modes are needed after coherence decreases from the spatial convolution.

From equations (15), (1) and (6) it follows that the overall degree of coherence may be given by the eigenvalues of the decomposition (Luis, 2007),

$$\mu_g^2 = \sum_n \lambda_n^2 / (\sum_n \lambda_n)^2. \quad (25)$$

For a perfectly coherent source, there is only a single λ equal to 1 and a single pure mode. For a perfectly incoherent source, an infinite number of modes are needed, and all λ_i approach zero. For the modal decomposition of the partially coherent undulator radiation which has been convolved over energy bandwidth and space, Fig. 9 shows how the the eigenvalues of the modal decomposition fall off for less and less heavily weighted modes.

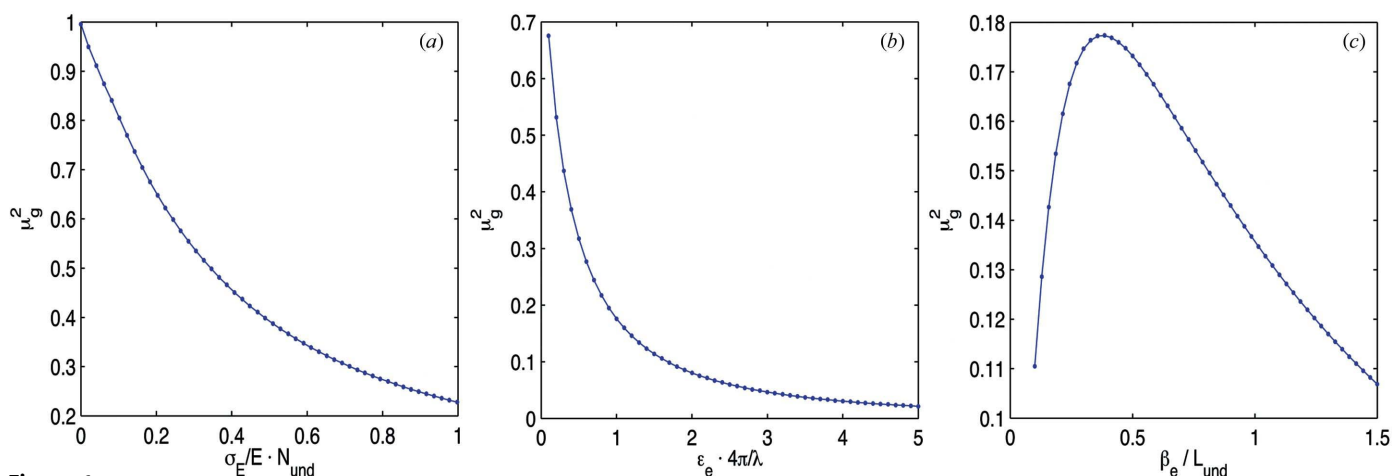


Figure 6 (a) Coherence versus electron energy spread with $\varepsilon_e = 0$. (b) Coherence versus electron bunch emittance with $\sigma_E = 0$, $\beta_e = \beta_{ph}$. (c) Coherence versus electron betatron function with $\sigma_E = 0$ and $\varepsilon_e = \lambda/(4\pi)$.

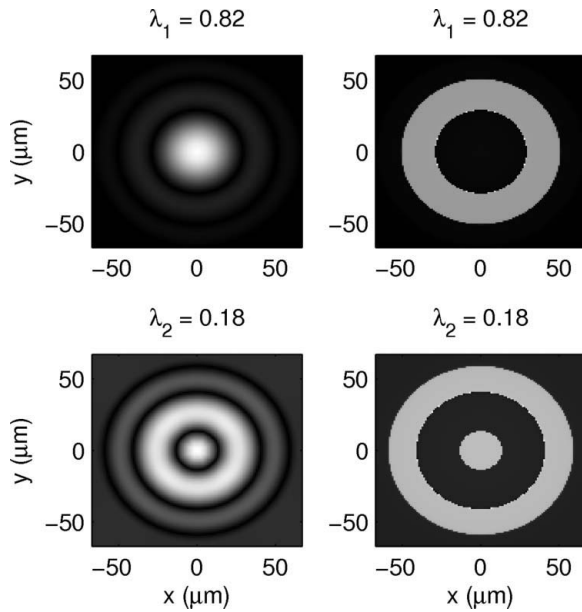


Figure 7
Amplitude (left) and complex phase (right) of the first two modes from decomposition after convolution over an electron bunch of non-zero energy bandwidth and zero emittance. The abrupt changes in phase correspond to phase transitions of π . $\mu_g^2 = 0.74$ for this radiation.

We expect that the eigenmodes of the CSD with corresponding WDF obeying equation (12) will have the form of equation (9). Figs. 7 and 8 demonstrate that this holds true in our example. Modes with a helical structure in their complex phase correspond to a non-zero orbital angular momentum. Notice that, for the decomposition in Fig. 8, the modes with helical phases come paired with a mode of opposite helicity, and the eigenvalues are almost equal for two paired modes such that the helicity is almost cancelled. This cancellation is not exact only because of numerical error. At high resolution, the eigenvalues of paired modes would become equal, reflecting the fact that planar undulator radiation has zero orbital angular momentum. We note that the phases shown in Fig. 8 are a particular gauge choice as any radial line can be chosen as $\varphi = 0$.

4. Conclusion

In this paper, we have provided computationally convenient alternatives to the full 4D WDF for sources of arbitrary degrees of coherence. For perfectly coherent sources, we showed that a 2D WDF can suffice for separable modes and for non-twisted rotationally symmetric sources. For twisted rotationally symmetric sources, we expanded the applicability of a dimension-reducing condition given by Alieva & Bastiaans (2000), equation (12), to all fields of the form (9). We found that this same formula could also be applied to perfectly incoherent sources exhibiting spatial rotational symmetry. In doing so, we have identified that a large class of rotationally symmetric systems of arbitrary degree of coher-

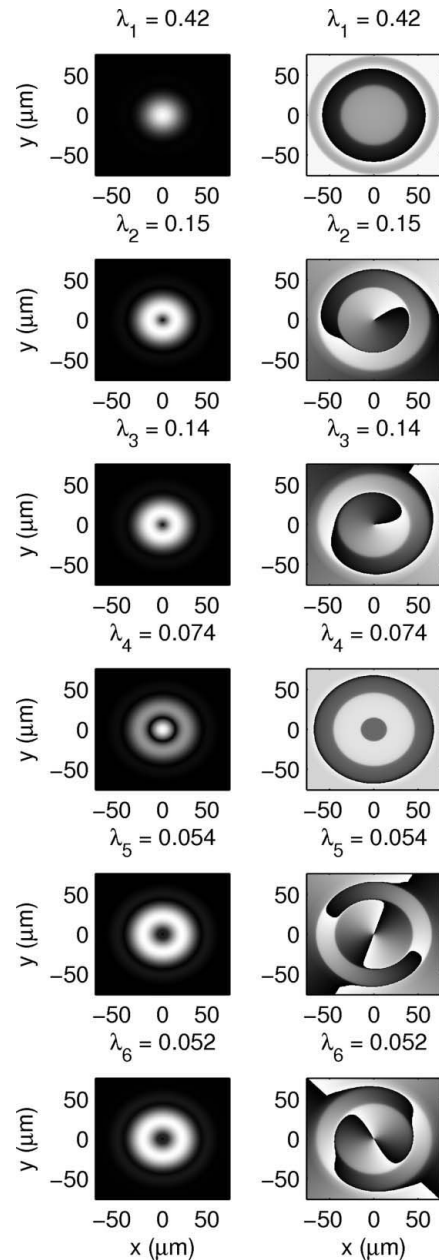


Figure 8
Amplitude (left) and complex phase (right) of the first six modes from decomposition after convolution over an electron bunch of non-zero energy bandwidth and non-zero emittance. $\mu_g^2 = 0.23$ for this radiation.

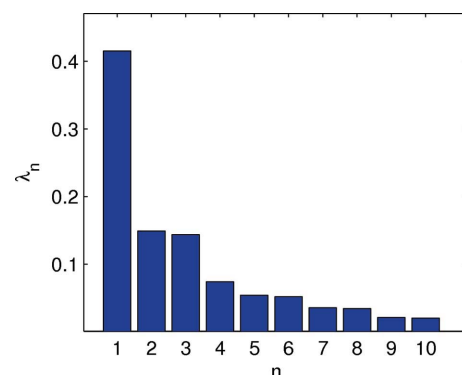


Figure 9
Eigenvalues of mode decomposition after convolution over energy and space.

ence can be represented by a WDF of three or fewer dimensions.

In §3, we modeled partially coherent undulator radiation as a convolution of a perfectly coherent photon source and a perfectly incoherent electron source. In three dimensions, we successfully performed the convolution. This gave us a complete physical picture of the synchrotron radiation in phase space, and also allowed us to examine how the overall degree of coherence of the radiation was effected by the electron bunch parameters. We diagonalized to CSD to recover the constituent eigenmodes, and we confirmed the prediction of equation (9) that the constituent modes of a rotationally symmetric partially coherent source should be states of definite orbital angular momentum. These modes can be conveniently applied to scattering experiment simulations for a realistic picture of how the partially coherent radiation interacts with matter.

There still remain a few open questions whose answers could enhance the presented methods. We have discussed that a non-twisted pure mode has only two degrees of freedom, but we were unable to find a useful 2D-reduced WDF. Does such a representation exist such that it is convenient and accessible (in the sense of computing the overall degree of coherence, for example)? When we performed mode decomposition, we resorted to using a 4D array to perform the diagonalization. Is there a way to perform decompositions of rotationally symmetric partially coherent sources entirely in 3D?

In summary, we have provided a viable numerical approach to phase space treatment of synchrotron radiation. Using reduced forms of the WDF, one may fully simulate rotationally symmetric light in phase space without large memory requirements and rigorously extract coherence and brightness properties of such sources.

APPENDIX A

Dimension-reducing condition for WDF

Here we prove that fields of the form equation (9) have WDFs obeying the symmetry equation (12). It is simplest to work in phase space polar coordinates as defined in equation (8). Plugging the expression for the fields into the definition of the WDF yields

$$B \begin{pmatrix} \rho_r \\ \varphi_r \\ \rho_\theta \\ \varphi_\theta \end{pmatrix} = B_0 \int d^2 \mathbf{r}' R(\rho_+) R(\rho_-) \times \exp\{i[\psi(\rho_-) - \psi(\rho_+)]\} \times \exp[i l(\varphi_- - \varphi_+)] \exp(i \mathbf{k} \mathbf{r} \cdot \boldsymbol{\theta}), \quad (26)$$

where we have defined

$$\rho_\pm \equiv |\mathbf{r} \pm \mathbf{r}'/2| = \left[\rho_r^2 + \frac{1}{4} \rho_r'^2 \pm \rho_r \rho_r' \cos(\varphi_r - \varphi_r') \right]^{1/2} \quad (27)$$

$$\tan(\varphi_\pm) \equiv (y \pm y'/2)/(x \pm x'/2)$$

and (ρ_r', φ_r') is a set of polar coordinates describing the integration variable \mathbf{r}' . Using some basic trigonometry, one can work out that

$$\varphi_- - \varphi_+ = \text{atan} \left[\frac{\rho_r \rho_r' \sin(\varphi_r - \varphi_r')}{\rho_r^2 - \frac{1}{4} \rho_r'^2} \right]. \quad (28)$$

So now everything in the integrand except the last exponential factor can be written as a function of only ρ_r, ρ_r' and $(\varphi_r - \varphi_r')$. Define

$$R_0(\rho_r, \rho_r', \varphi_r - \varphi_r') \equiv R(\rho_-) R(\rho_+) \exp\{i[\psi(\rho_-) - \psi(\rho_+)]\} \times \exp[i l(\varphi_- - \varphi_+)]. \quad (29)$$

Putting this all together the WDF expression has become

$$B \begin{pmatrix} \rho_r \\ \varphi_r \\ \rho_\theta \\ \varphi_\theta \end{pmatrix} = B_0 \int d^2 \mathbf{r}' R_0(\rho_r, \rho_r', \varphi_r - \varphi_r') \times \exp[\rho_r' \rho_\theta \cos(\varphi_r' - \varphi_\theta)]. \quad (30)$$

In polar coordinates, equation (12) takes the form

$$B \begin{pmatrix} \rho_r \\ \varphi_r + \gamma \\ \rho_\theta \\ \varphi_\theta + \gamma \end{pmatrix} = B \begin{pmatrix} \rho_r \\ \varphi_r \\ \rho_\theta \\ \varphi_\theta \end{pmatrix}. \quad (31)$$

Then evaluating the left-hand side of (31) using (30) we find

$$B \begin{pmatrix} \rho_r \\ \varphi_r + \gamma \\ \rho_\theta \\ \varphi_\theta + \gamma \end{pmatrix} = B_0 \int d^2 \mathbf{r}' R_0[\rho_r, \rho_r', \varphi_r - (\varphi_r' - \gamma)] \times \exp\{\rho_r' \rho_\theta \cos[(\varphi_r' - \gamma) - \varphi_\theta]\}. \quad (32)$$

We then make a substitution for the angular integration variable $\varphi_r'' = \varphi_r' - \gamma$, and we are left with the dimension-reducing expression equation (31). QED.

APPENDIX B

Dimension-reducing condition for CSD

For systems with WDF obeying equation (12), we can derive a corresponding dimension-reducing condition for the CSD. It is simplest to show this in Cartesian coordinates. The CSD is computed from the WDF using equation (3),

$$W \begin{pmatrix} x_1 \\ y_1 \\ x_2 \\ y_2 \end{pmatrix} = \int d^2 \boldsymbol{\theta} B \begin{pmatrix} (x_1 + x_2)/2 \\ (y_1 + y_2)/2 \\ \theta_x \\ \theta_y \end{pmatrix} \times \exp \left[ik \begin{pmatrix} \theta_x \\ \theta_y \end{pmatrix} \cdot \begin{pmatrix} x_1 - x_2 \\ y_1 - y_2 \end{pmatrix} \right]. \quad (33)$$

The coordinates have been placed into columns to condense notation. The expression in the exponent is a dot product

between two column vectors. We can apply equation (12) to the WDF in the integrand,

$$W \begin{pmatrix} x_1 \\ y_1 \\ x_2 \\ y_2 \end{pmatrix} = \int d^2\theta B \begin{pmatrix} [(x_1 + x_2)/2] \cos \gamma - [(y_1 + y_2)/2] \sin \gamma \\ [(y_1 + y_2)/2] \cos \gamma + [(x_1 + x_2)/2] \sin \gamma \\ \theta_x \cos \gamma - \theta_y \sin \gamma \\ \theta_y \cos \gamma + \theta_x \sin \gamma \end{pmatrix} \times \exp \left[ik \begin{pmatrix} \theta_x \\ \theta_y \end{pmatrix} \cdot \begin{pmatrix} x_1 - x_2 \\ y_1 - y_2 \end{pmatrix} \right]. \quad (34)$$

Now we make a substitution of integration variables,

$$\begin{aligned} \theta'_x &= \theta_x \cos \gamma - \theta_y \sin \gamma \\ \theta'_y &= \theta_y \cos \gamma + \theta_x \sin \gamma. \end{aligned} \quad (35)$$

Note that this substitution is just a simple rotation, and so the Jacobian is unity. Applying the substitution, we find

$$\begin{aligned} W \begin{pmatrix} x_1 \\ y_1 \\ x_2 \\ y_2 \end{pmatrix} &= \int d^2\theta' B \begin{pmatrix} [(x_1 + x_2)/2] \cos \gamma - [(y_1 + y_2)/2] \sin \gamma \\ [(y_1 + y_2)/2] \cos \gamma + [(x_1 + x_2)/2] \sin \gamma \\ \theta'_x \\ \theta'_y \end{pmatrix} \\ &\times \exp \left[ik \begin{pmatrix} \theta'_x \cos \gamma + \theta'_y \sin \gamma \\ \theta'_y \cos \gamma - \theta'_x \sin \gamma \end{pmatrix} \cdot \begin{pmatrix} x_1 - x_2 \\ y_1 - y_2 \end{pmatrix} \right] \\ &= \int d^2\theta' B \begin{pmatrix} [(x_1 \cos \gamma - y_1 \sin \gamma)/2] + [(x_2 \cos \gamma - y_2 \sin \gamma)/2] \\ [(y_1 \cos \gamma + x_1 \sin \gamma)/2] + [(y_2 \cos \gamma + x_2 \sin \gamma)/2] \\ \theta'_x \\ \theta'_y \end{pmatrix} \\ &\times \exp \left\{ ik \begin{pmatrix} \theta'_x \\ \theta'_y \end{pmatrix} \cdot \begin{pmatrix} [x_1 \cos \gamma - y_1 \sin \gamma] - [x_2 \cos \gamma - y_2 \sin \gamma] \\ [y_1 \cos \gamma + x_1 \sin \gamma] - [y_2 \cos \gamma + x_2 \sin \gamma] \end{pmatrix} \right\}. \end{aligned} \quad (36)$$

The last expression is simply equation (3) evaluated at new arguments. Thus this expression yields the dimension-reducing expression

$$W \begin{pmatrix} x_1 \\ y_1 \\ x_2 \\ y_2 \end{pmatrix} = W \begin{pmatrix} x_1 \cos \gamma - y_1 \sin \gamma \\ y_1 \cos \gamma + x_1 \sin \gamma \\ x_2 \cos \gamma - y_2 \sin \gamma \\ y_2 \cos \gamma + x_2 \sin \gamma \end{pmatrix}. \quad (37)$$

This work supported by the National Science Foundation (grant No. DMR-0807731).

References

- Afanasev, A. & Mikhailichenko, A. (2011). ArXiv e-print 1109.1603.
 Agarwal, G. S. & Simon, R. (2000). *Opt. Lett.* **25**, 1379–1381.
 Alieva, T. & Bastiaans, M. J. (2000). *J. Opt. Soc. Am. A*, **17**, 2319–2323.
 Bartnik, A. *et al.* (2013). *Cornell ERL: Project Definition Design Report*, edited by G. H. Hoffstaetter, S. M. Gruner and M. Tigner. Cornell High Energy Synchrotron Source, Ithaca, New York, USA.
 Bazarov, I. V. (2012). *Phys. Rev. ST Accel. Beams*, **15**, 050703.
 Bazarov, I. V. & Gasbarro, A. D. (2012). *Proceedings of the 2012 International Particle Accelerator Conference*, paper WEOBB03.
 Borland, M. (2013). *J. Phys. Conf. Ser.* **425**, 042016.
 Chubar, O., Elleaume, P., Kuznetsov, S. & Snigirev, A. A. (2002). *Proc. SPIE*, **4769**, 145.
 Geloni, G., Saldin, E., Schneidmiller, E. & Yurkov, M. (2008). *Nucl. Instrum. Methods Phys. Res. A*, **588**, 463–493.
 Goodman, J. W. (2000). *Statistical Optics*. New York: Wiley-Interscience.
 Kim, K.-J. (1986). *Nucl. Instrum. Methods Phys. Res. A*, **246**, 71–76.
 Kim, K.-J. (1989). *AIP Conf. Proc.* **184**, 565–632.
 Luis, A. (2005). *Opt. Commun.* **246**, 437–443.
 Luis, A. (2007). *J. Opt. Soc. Am. A*, **24**, 2070–2074.
 Sakurai, J. J. & Napolitano, J. J. (2010). *Modern Quantum Mechanics*, 2nd ed. New York: Addison-Wesley.
 Smithey, D. T., Beck, M. & Raymer, M. G. (1993). *Phys. Rev. Lett.* **70**, 1244.
 Tran, C. Q. (2007). *Phys. Rev. Lett.* **98**, 224801.
 Vartanyants, I. A. & Singer, A. (2010). *New J. Phys.* **12**, 035004.